Published in final edited form as:

JACC Cardiovasc Imaging. 2022 August ; 15(8): 1391–1405. doi:10.1016/j.jcmg.2021.07.010.

Accuracy of Cardiac Magnetic Resonance Imaging in Diagnosing Pediatric Cardiac Masses:

A Multicenter Study

Rebecca S. Beroukhim, MD[a], **Sunil Ghelani, MD**[a], **Ravi Ashwath, MD**[b], **Sowmya Balasubramanian, MD**[c], **David M. Biko, MD**[d], **Sujatha Buddhe, MBBS, MS**[e], **M. Jay Campbell, MD, MHA**[f], **Russell Cross, MD**[g], **Pierluigi Festa, MD**[h], **Lindsay Griffin, MD**[i], **Heynric Grotenhuis, MD, PhD**[j], **Keren Hasbani, MD**[k], **Sassan Hashemi, MD**[l], **Sanjeet Hegde, MD, PhD**[m], **Tarique Hussain, MD, PhD**[n], **Supriya Jain, MD**[o], **Maria Kiaffas, MD**[p], **Shelby Kutty, MD, MS, PhD**[q,r], **Christopher Z. Lam, MD**[s], **Gabriela Liberato, MD**[t], **Anthony Merlocco, MD**[u], **Nilanjana Misra, MD**[v], **Katie L. Mowers, MD**[c,w], **Juan Carlos Muniz, MD**[x], **Arni Nutting, MD**[y], **David A. Parra, MD**[z], **Jyoti K. Patel, MD**[aa], **Antonio R. Perez-Atayde, MD, PhD**[a], **Deepa Prasad, MD**[bb], **Carlos F. Rosental, MD**[cc], **Amee Shah, MD**[dd], **Margaret M. Samyn, MD**[ee], **Lynn A. Sleeper, ScD**[a], **Timothy Slesnick, MD**[l], **Emanuela Valsangiacomo, MD**[ff], **Tal Geva, MD**[a]

[a]Boston Children's Hospital, Boston, Massachusetts, USA;

[b]University of Iowa Stead Family Children's Hospital, Iowa City, Iowa, USA;

[c]CS Mott Children's Hospital, Ann Arbor, Michigan, USA;

[d]Children's Hospital of Philadelphia, Philadelphia, Pennsylvania, USA;

[e]Seattle Children's Hospital, Seattle, Washington, USA;

[f]Duke Children's Hospital, Durham, North Carolina, USA;

[g]Children's National Medical Center, Washington, DC, USA;

[h]Fondazione G. Monasterio C.N.R. Regione Toscana, Pisa, Italy;

[i]Ann & Robert H Lurie Children's Hospital of Chicago, Chicago, Illinois, USA;

[j]University of Utrecht, Utrecht, the Netherlands;

[k]Dell Children's Medical Center, Austin, Texas, USA;

[l]Children's Healthcare of Atlanta, Atlanta, Georgia, USA;

[m]Rady Children's Hospital San Diego, San Diego, California, USA;

[n]Children's Medical Center Dallas, Dallas, Texas, USA;

ADDRESS FOR CORRESPONDENCE: Dr Rebecca S. Beroukhim, Department of Cardiology, Boston Children's Hospital, 300 Longwood Avenue, Boston, Massachusetts 02115, USA. rebecca.beroukhim@cardio.chboston.org. Twitter: @dr_rebecca_b.

The authors attest they are in compliance with human studies committees and animal welfare regulations of the authors' institutions and Food and Drug Administration guidelines, including patient consent where appropriate. For more information, visit the Author Center.

FUNDING SUPPORT AND AUTHOR DISCLOSURES

The authors have reported that they have no relationships relevant to the contents of this paper to disclose.

APPENDIX For supplemental tables and figures, please see the online version of this paper.

[o]Maria Fareri Children's Hospital at Westchester Medical Center, Valhalla, New York, USA;

[p]Children's Mercy Hospital, Kansas City, Missouri, USA;

[q]Johns Hopkins Children's Center, Baltimore, Maryland, USA;

[r]Children's Hospital and Medical Center, Omaha, Nebraska, USA;

[s]Hospital for Sick Children, Toronto, Canada;

[t]Heart Institute, InCor, Sao Paulo, Brazil;

[u]Le Bonheur Children's Hospital, Memphis, Tennessee, USA;

[v]Cohen Children's Medical Center of New York, Northwell Health, New Hyde Park, New York, USA;

[w]St Louis Children's Hospital, St Louis, Missouri, USA;

[x]Nicklaus Children's Hospital, Miami, Florida, USA;

[y]Medical University of South Carolina, Charleston, South Carolina, USA;

[z]Vanderbilt Children's Hospital, Nashville, Tennessee, USA;

[aa]Riley Children's Hospital, Indianapolis, Indiana, USA;

[bb]Banner Children's Hospital, Mesa, Arizona, USA;

[cc]Hospital Pediatria Garrahan, Buenos Aires, Argentina;

[dd]Children's Hospital of New York, New York, New York, USA;

[ee]Medical Collect of Wisconsin/Children's Wisconsin, Milwaukee, Wisconsin, USA;

[ff]University Children's Hospital Zurich, Zurich, Switzerland.

Abstract

BACKGROUND—After diagnosis of a cardiac mass, clinicians must weigh the benefits and risks of ascertaining a tissue diagnosis. Limited data are available on the accuracy of previously developed noninvasive pediatric cardiac magnetic resonance (CMR)-based diagnostic criteria.

OBJECTIVES—The goals of this study were to: 1) evaluate the CMR characteristics of pediatric cardiac masses from a large international cohort; 2) test the accuracy of previously developed CMR-based diagnostic criteria; and 3) expand diagnostic criteria using new information.

METHODS—CMR studies (children 0–18 years of age) with confirmatory histological and/or genetic diagnosis were analyzed by 2 reviewers, without knowledge of prior diagnosis. Diagnostic accuracy was graded as: 1) single correct diagnosis; 2) correct diagnosis among a differential; or 3) incorrect diagnosis.

RESULTS—Of 213 cases, 174 (82%) had diagnoses that were represented in the previously published diagnostic criteria. In 70% of 174 cases, both reviewers achieved a single correct diagnosis (94% of fibromas, 71% of rhabdomyomas, and 50% of myxomas). When ≤2 differential diagnoses were included, both reviewers reached a correct diagnosis in 86% of cases. Of 29 malignant tumors, both reviewers indicated malignancy as a single diagnosis in 52% of cases.

Including ≤2 differential diagnoses, both reviewers indicated malignancy in 83% of cases. Of 6 CMR sequences examined, acquisition of first-pass perfusion and late gadolinium enhancement were independently associated with a higher likelihood of a single correct diagnosis.

CONCLUSIONS—CMR of cardiac masses in children leads to an accurate diagnosis in most cases. A comprehensive imaging protocol is associated with higher diagnostic accuracy.

Keywords

cardiac mass; cardiac tumor; cardiac magnetic resonance; pediatric

The signs, symptoms, and prognosis of cardiac masses in children vary depending on their location and histology, and in many instances, the clinical course is benign.[1] Upon recognition of a cardiac mass, clinicians must use available data to weigh the benefits of a confirmed histological diagnosis against the risks of surgical or transcatheter biopsy to obtain a tissue sample.[2] Thus, accurate and reproducible noninvasive methods of diagnosis are needed to avoid the use of invasive biopsy in situations where masses are benign and the expected clinical course does not warrant intervention. Cardiac magnetic resonance (CMR) imaging provides valuable data on the location, size, and tissue characteristics of masses. In 2011, we published the results of a multicenter study describing CMR-based diagnostic criteria in 78 children with pediatric cardiac masses.[3] These original diagnostic criteria have several limitations, including a lack of validation on an independent cohort and a lack of precision in the diagnosis of rare cardiac masses. Therefore, we conducted this study to test the accuracy of the original diagnostic criteria on a new cohort of patients, to refine the CMR diagnostic criteria based on a new large data set from a large multicenter cohort, and to expand the experience by adding rare masses.

METHODS

PATIENTS.

This was a retrospective multicenter study of pediatric cardiac masses. Investigators at the CMR core laboratory at Boston Children's Hospital solicited cases from an international group of pediatric cardiac imaging centers for patients fulfilling the following criteria: 1) aged ≤18 years at the time of diagnosis; 2) CMR of cardiac mass; and 3) histological or genetic diagnosis identifying mass type.

Submissions of mediastinal masses in close proximity to the heart were included because the investigators assumed there was uncertainty about the origin of the mass at the time of image acquisition. The following cases were excluded: 1) inability to identify a mass at the core laboratory because of image artifacts; and 2) case inclusion in the prior published study.[3] The study was approved by the Scientific Review Committee of the Department of Cardiology, and the requirement for informed consent was waived by the Boston Children's Hospital Committee on Clinical Investigation. Contributing centers followed the policies of their respective institutional review boards. Data transfer agreements were obtained between the Boston Children's Hospital Clinical Trials Business Office and each respective institution to ensure that data sharing complied with all applicable international, federal, state, and local laws.

DATA COLLECTION.

All patient identifying information was removed at the contributing institutions, and each case was assigned a unique study number. The submitting institutions completed case information forms in REDCap (Research Electronic Data Capture) tools hosted at Boston Children's Hospital. Each submitting institution was assigned to a data access group so that only investigators from the submitting institution and core laboratory had access to each group. The following demographic and clinical information were recorded: 1) center name and location; 2) patient demographics at the time of CMR; 3) presenting signs and symptoms, comorbid conditions, and other disease diagnoses; 4) CMR technical data; 5) adverse events attributable or possibly attributable to CMR; 6) source of tissue; 7) final pathologic diagnosis; 8) treatment; and 9) age and clinical status at latest follow-up. A deidentified digital copy of the CMR was submitted to the core laboratory for review.

CMR IMAGE ANALYSIS.

CMR images were reviewed for mass characteristics by a single investigator (RSB) as previously described.[3] Signal intensity ratio was defined as the signal intensity of the mass relative to adjacent, uninvolved myocardium. In addition, the largest linear mass dimension was indexed to cardiac length in a 4-chamber view (Figure 1A). Fibroma late gadolinium enhancement (LGE) pattern was defined as hyperenhancement with patchy dark areas (Figure 1B). Hemodynamic impact was defined as any impairment of normal cardiac physiology as a result of the mass assessed by CMR and/or other diagnostic modalities (eg, echocardiography) as reported by the submitting center. Hemodynamic impairment was also assessed qualitatively and included obstruction to ventricular inflow or outflow (anatomical narrowing with diastolic or systolic flow disturbance on cine imaging), compression of lung tissue and/or pulmonary vein accompanied by abnormal lung perfusion, more than mild mitral or tricuspid regurgitation, pericardial effusion with features of tamponade (atrial collapse or diastolic ventricular collapse), and ventricular dysfunction defined as ejection fraction >2 SDs below normal.

Infiltrative pattern was defined as: 1) crossing a tissue plane (such as the valve annulus); 2) involving both cardiac and extracardiac structures; and/or 3) the appearance of linear growth through a large vessel such as the superior or inferior vena cava. Using previously developed diagnostic criteria, 2 investigators (R.S.B. [14 years of CMR experience]; and S.G. [4 years of CMR experience]) independently reviewed each case and assigned it a most likely single diagnosis or a set of differential diagnoses. Table 1 of the prior publication was used as a reference, and characteristics marked with an asterisk were considered the minimum necessary criteria for diagnosis.[3] Based on the diagnostic criteria, options included: 1) fibroelastoma; 2) fibroma; 3) Purkinje cell tumor/histiocytoid cardiomyopathy; 4) lipoma, 5) myxoma; 6) pleuropericardial cyst; 7) rhabdomyoma; 8) teratoma; 9) thrombus; 10) vascular; 11) malignant; and 12) other. To simulate the clinical scenario, investigators had access to clinical patient characteristics at the time of image analysis (including a prior history of malignancy) but were blinded to any prior genetic diagnosis and the final tissue diagnosis. The suspected single or differential diagnoses were assessed for accuracy against histology or genetic diagnosis. For mass types that were included in the previously published diagnostic criteria, accuracy was graded as: 1) single correct diagnosis; 2) correct diagnosis

among a differential; and 3) incorrect diagnosis. A study comprehensiveness score was calculated based on the number of sequences performed (a maximum score of 6) for: 1) cine steady-state free precession (SSFP); 2) T_1-weighted turbo spin echo; 3) T_2-weighted turbo spin echo; 4) fat-suppressed imaging; 5) first-pass perfusion; and 6) LGE imaging. Using data from this study and cases from the published reports, updates to the diagnostic criteria were developed.

STATISTICAL ANALYSIS.

Continuous variables were summarized as median (IQR). Categorical variables were described in counts (percentages). The frequency and percentage, gross characteristics, and CMR-based tissue characteristics of each mass type (according to final histological or genetic diagnosis) are reported. We report the percent agreement between the 2 independent reviewers with exact binomial 95% CIs. A Fisher exact test was performed to compare comprehensiveness score and diagnostic accuracy. Non-normally distributed continuous variables were categorized according to data tertile for logistic regression analyses except first-pass perfusion imaging data, which was divided into a binary variable with signal intensity ratios of <1 vs ≥1. Univariate and multivariable logistic regressions were used to identify which sequences were associated with a higher odds of single correct diagnosis and which patient and mass characteristics were associated with specific mass types. Firth bias adjustment was applied to minimize bias from small sample sizes for each mass type. Genetic diagnoses were excluded from logistic regression analyses because they were used to define the outcome variable (final pathologic diagnosis) in certain cases. Univariate and multivariable Cox proportional hazards regressions were used to identify which variables (excluding the final diagnosis) were associated with a higher hazard of death. To identify any differential predictors of death for malignant and nonmalignant tumors, models with an interaction term between malignancy and each predictor were fit. Because of the large number of predictor variables and higher likelihood of false discovery, candidate variables for multivariable logistic regression and multivariable Cox proportional hazards regression were identified based on a value of $P < 0.10$ from univariate regression. All mass characteristics associated with mass type by univariate regression ($P < 0.05$) were included in the updated diagnostic table. All tests were performed with 2-sided type I error rate of 0.05. Data analyses were performed with SAS software, version 9.4 (SAS Institute, Inc).

RESULTS

PATIENTS AND CLINICAL PRESENTATION.

Cases (n = 232) were submitted from an international group of 31 imaging centers from 6 countries. Of those, 19 were excluded for the following reasons: lack of histological diagnosis (n = 10), no CMR images submitted (n = 3), no visible mass on CMR images (n = 3), duplicate submission from prior study (n = 2), and aged >18 years at the time of diagnosis (n = 1). The remaining 213 cases comprised the study cohort. Table 1 summarizes patient demographics and clinical characteristics. Prenatal diagnosis of a cardiac mass (18%) was reported for 4 mass types: fibroma (n = 15), rhabdomyoma (n = 18), teratoma (n = 4), and hemangioma (n = 1). Aside from prenatal diagnosis, the most common clinical presentations were respiratory symptoms (19%), arrhythmia (19%), and heart murmur

(15%). Hemodynamic impact was noted in 79 (37%) patients and included obstruction to mitral inflow in 11 (5%), obstruction to tricuspid inflow in 15 (7%), obstruction to left ventricular outflow in 12 (6%), obstruction to right ventricular outflow in 22 (10%), superior or inferior vena cava obstruction in 8 (4%), cardiac compression in 6 (3%), mitral or tricuspid regurgitation in 6 (3%), evidence of tamponade from large pericardial effusion in 4 (2%), lung compression in 3 (1%), pulmonary venous obstruction in 3 (1%), and left ventricular dysfunction in 2 (1%). Genetic diagnoses associated with mass type included Gorlin syndrome in association with fibroma (n = 11), tuberous sclerosis in association with rhabdomyoma (n = 28) and myocardial fatty deposits (n = 6), Carney complex in association with myxoma (n = 4), and neurofibromatosis in association with neurofibroma (n = 2).

The final pathologic diagnosis was confirmed by tissue biopsy in 162 (76%), genetic diagnosis in 43 (20%), and both tissue biopsy and genetic diagnosis in 8 (4%) patients. Of the 170 patients with a tissue diagnosis, 158 (93%) were obtained by surgery (biopsy or resection), 7 (4%) by transcatheter biopsy, 2 (1%) from biopsy of an explanted heart, 1 from cytology of a pericardial/pleural effusion, and 1 from transbronchial biopsy. Of the 9 attempted transcatheter biopsies, none had complications, and 7 were technically successful at obtaining tissue for pathologic analysis (Supplemental Table 1). Complications of surgical resection were reported in 4 patients, including aortic valvuloplasty after fibroelastoma removal (n = 1), mitral valvuloplasty after hemangioma removal from the mitral valve (n = 1), left coronary artery injury requiring left ventricular assist device after teratoma resection (n = 1), and left coronary artery injury associated with removal of synovial sarcoma (n = 1).

Of 163 patients with available follow-up data, the median length of follow-up was 7 years (IQR: 3–14 years). Of those, 18 patients (11%) were deceased during follow-up, including 11 patients with malignant tumors, 2 with teratomas, 1 with a fibroma, 1 with a rhabdomyoma, 1 with a thrombus, 1 with an inflammatory myofibroblastic tumor, and 1 with a fibroelastoma. Clinical data on the 29 patients with malignant tumors are shown in Supplemental Table 2. Of the malignant tumors, patient age at diagnosis ranged from 44 days to 18 years, and treatment included chemotherapy, radiation, and/or surgical resection. Although mortality was significantly higher in patients with malignant tumors, 5 of the 22 patients with follow-up data were reported to be “alive and asymptomatic” between 4 and 7 years following CMR (Figure 2). By univariate Cox regression, excluding pathologic or genetic diagnosis, multiple clinical factors and imaging characteristics were associated with an increased hazard of death among the patients with follow-up data (n = 163) (Supplemental Table 3). Four factors were independently associated with an increased hazard of death: fetal diagnosis (HR: 7.9; 95% CI: 1.6–39.5), pericardial effusion (HR: 3.5; 95% CI: 1.2–9.9), hemodynamic impact (HR: 4.0; 95% CI: 1.2–12.3), and fever at presentation (HR: 7.2; 95% CI: 1.6–33.8). No malignant mass was identified prenatally. There were no unique risk factors for death between patients with malignant versus benign tumors.

TECHNICAL ASPECTS OF CMR.

CMR technical characteristics are shown in Supplemental Table 4. Technical difficulties were reported in 7 studies, including inability to hold breath (n = 4), metallic artifact (n =

2), and contraindication to gadolinium contrast because of acute renal failure (n = 1). Image quality was rated as good or very good in most cases (91%). Out of 6 sequences measured (cine SSFP, T_1-weighted turbo spin echo, T_2-weighted turbo spin echo, fat-suppressed imaging, first-pass perfusion, and LGE imaging), the median comprehensiveness score was 5 (IQR: 4–5). The proportion of cases with LGE imaging was significantly increased compared with the prior study (78% vs 58%; $P < 0.001$).

DIAGNOSTIC ACCURACY.

Diagnostic accuracy was assess for mass types that were represented in the original diagnostic criteria (n = 174) (Figure 3). Mass types that were not represented in the original diagnostic criteria (n = 39) can be found in Supplemental Table 5. Of 12 available diagnosis options, the median number of diagnosis selections per case was 1 for both reviewers. In 70% of cases (95% CI: 63%−77%), both reviewers selected a single correct diagnosis. Including ≤2 differential diagnoses, both reviewers reached a correct diagnosis in 86% of cases (95% CI: 80%−91%) (Figure 4). Of the cases with malignant tumors (n = 29), 13 (45%) had a prior history of malignancy. In 52% of cases (95% CI: 34%−70%), both reviewers had a single correct diagnosis. Including ≤2 differential diagnoses, both reviewers reached a correct diagnosis in 83% of cases (95% CI: 69%−97%) (Figure 4). One mass that was incorrectly diagnosed as benign by reviewer 1 was also incorrectly diagnosed on the clinical study report (Figure 5).

Among the nonmalignant masses represented by the original diagnostic criteria (n = 145), 2 (1%) had a prior history of malignancy, including 1 myxoma and 1 fibroma with Gorlin syndrome. Reviewer 1 indicated malignancy among a differential diagnosis in 12 (8%) nonmalignant masses, including 4 fibromas, 1 hemangioma, 3 myxomas, 2 rhabdomyomas, 1 teratoma, and 1 thrombus (Supplemental Figure 1). Reviewer 2 indicated malignancy among a differential diagnosis in 7 (5%) nonmalignant masses, including 2 myxomas, 3 rhabdomyomas, 1 teratoma, and 1 thrombus (Supplemental Figures 2 and 3).

STUDY COMPREHENSIVENESS.

Study comprehensiveness was higher among cases in which both readers came to a single correct diagnosis (median comprehensiveness score: 6 [IQR: 5–6] vs 5 [IQR: 3–6]; $P = 0.005$). Of the 6 imaging sequences, acquisition of first-pass perfusion and LGE imaging were independently associated with a higher likelihood of a single correct diagnosis (first-pass perfusion odds ratio [OR]: 2.0; 95% CI: 1.1–3.4; $P = 0.016$; LGE imaging OR: 1.8; 95% CI: 1.1–2.9; $P = 0.017$).

CMR CHARACTERISTICS OF CARDIAC MASSES.

Mass types and their characteristics are listed in Supplemental Table 5, and factors significantly associated with mass type from univariate analysis are shown in Supplemental Table 6. Independent predictors of mass type from multivariable logistic regression analyses are shown in Table 2. Although larger tumor size (mass-to-cardiac ratio: >0.60) and higher cine SSFP intensity ratio were among the independent predictors of fibroma, we also found that older age in patients with fibroma correlated with smaller tumor size ($r = 0.50$; $P < 0.001$), lower cine SSFP intensity ratio ($r = 0.30$; $P = 0.007$), and lower T_2 intensity

ratio ($r = 0.50$; $P < 0.001$). In addition, we found notable characteristics of several rare mass types. Compared to other masses, all 7 fatty deposits in tuberous sclerosis complex had fat content (100% vs 8%), all 5 thrombi were endocardial in location (100% vs 22%), all 3 papillary fibroelastomas were endocardial in location (100% vs 23%), 3 of the 5 benign myofibroblastic masses were found in an outflow tract (60% vs 7%), and both neurofibromas were found in the posterior mediastinum (100% vs 2%). Regarding symptoms, 2 of the 3 children with Rosai Dorfman disease had chest pain (67% vs 7%). In addition, both patients with paraganglioma had a history of arrhythmia (100% vs 18%), and both paragangliomas had a first-pass perfusion intensity ratio of >1 (100% vs 10%). Proposed updates to the original diagnostic criteria are listed in Table 3.

DISCUSSION

With the availability of multiple tissue characterization imaging sequences, CMR has unique strengths in the noninvasive diagnosis of cardiac masses. In a prior publication, we developed CMR-based diagnostic criteria with key features associated with several mass types.[3] Herein, we present the largest multicenter experience of CMR characteristics of 213 pediatric cardiac masses, all with diagnostic confirmation based on tissue or genetic diagnosis. Our results validate the main findings of the previous diagnostic table regarding the 7 most common types of cardiac tumors in children (rhabdomyoma, fibroma, myxoma, hemangioma, teratoma, and malignant). Moreover, the current study expands our knowledge over the prior publication by: 1) providing a data-driven analysis of independent predictors for several of the common mass types; 2) providing a comprehensive table of mass characteristics, including 39 (18%) cases that were not represented in the original diagnostic criteria (Supplemental Table 5); 3) demonstrating an incremental benefit of evaluating mass characteristics and clinical variables over CMR-based characteristics alone (particularly for malignant tumors, myxomas, and teratomas) (Table 2); and 4) providing a clinically useful classification system (Table 3). Because cardiac masses are rare, with a wide range in histology and clinical behavior, individual pediatric centers often have limited experience in their CMR evaluation. This publication can potentially improve practice by providing diagnostic tools to clinicians with wide ranges in expertise. In the following sections, we discuss the most common types of cardiac tumors and masses examined by CMR, followed by updated diagnostic criteria and a recommended approach to the evaluation of cardiac masses in children (Figure 6).

FIBROMA.

A large number of fibroma cases (n = 73) were included, allowing for the identification of several independent predictors of tumor type (Table 2). Furthermore, both reviewers had a high percentage of single correct diagnosis in the fibroma studies (97% when LGE imaging was performed), demonstrating that CMR has a high diagnostic accuracy for this tumor. Based on these data, we stipulate that identification of fibroma by comprehensive CMR examination with LGE imaging may allow clinicians to avoid the use of diagnostic biopsy in almost all cases. The age-related decrease in cine SSFP and T_2 intensity ratio observed in this study mirrors findings on pathologic examination of surgically resected fibromas, which

have demonstrated higher collagen density and less interdigitating myocardium in fibromas resected from older patients.[4]

RHABDOMYOMA.

We identified several independent predictors of rhabdomyoma, including younger age, cine SSFP intensity ratio of <1.6, and LGE intensity ratio of <1.4. Although these variables were strongly associated with the diagnosis, reviewers had a lower accuracy for the diagnosis of rhabdomyoma compared to fibroma (69% single correct diagnosis and 94% correct including differential) (Figure 3). We hypothesize that the lower accuracy is associated with referral of atypical rhabdomyomas for CMR, as well as a higher proportion of cases without LGE imaging. Typically, rhabdomyomas present as multiple tumors in the fetus or neonate, and the tumors regress as children age.[5] The identification of multiple masses by echocardiogram, and a genetic diagnosis of tuberous sclerosis are often sufficient for the diagnosis of rhabdomyoma, without the need for CMR.[6] In the current study, 11 of 32 patients were older than 1 year at the time of CMR (the oldest was 8 years), and 72% of patients had an atypical solitary mass, reflecting a referral bias. Furthermore, a high proportion of rhabdomyoma cases in our series had no LGE imaging, implying that the diagnosis of rhabdomyoma was known before CMR (31% rhabdomyomas without LGE imaging vs 18% fibromas without LGE imaging).

MYXOMA.

Although myxomas classically form as pedunculated tumors attached to the atrial septum, they may be challenging to diagnose because they can “mimic’” other mass types. Prior studies have shown variable signal characteristics of myxoma on CMR, which are thought to be related to the high frequency of myxomatous elements, chronic hemorrhage, calcification, fibrosis, and cystic changes.[7] Although we found 2 independent predictors of myxoma (endocardial location and cine SSFP intensity ratio of >1.6), reviewers were able to reach a single correct diagnosis in only approximately 50% of cases. Selection bias likely played a role, in that patients with large atrial myxomas will often proceed to surgical removal without a diagnostic CMR because of the potential for obstruction or embolization.

MALIGNANT TUMORS.

In our cohort of 29 malignant tumors, reviewers suspected malignancy as a single diagnosis in 71% of cases. These findings are similar to prior adult studies that have shown a single correct diagnosis of malignancy in 79% to 89% of malignant cases.[8] None of the independent predictors of malignancy involved tissue characterization sequences; instead, the following features were strongly associated with a malignant cardiac tumor: 1) history of malignancy; 2) infiltrative appearance; and 3) chest pain. One notable limitation of CMR is the inability to detect metabolic activity. In studies of adult cardiac tumors, evidence of metabolic activity by ^{18}F-fluorodeoxyglucose (^{18}F-FDG) positron emission tomography (PET) has been associated with an increased likelihood of malignancy.[9] Thus, in situations where the potential for malignancy remains unknown, clinicians may consider ^{18}F-FDG PET to decide whether biopsy is indicated.

VASCULAR ANOMALIES.

The current study expands our knowledge about rare vascular anomalies, including hemangioendothelioma, glomus tumor, and vascular malformations. We recommend following the 2018 International Society for the Study of Vascular Anomalies (ISSVA) classification system for vascular anomalies.[10] It is important to note that within the ISSVA classification system, the subgroup of vascular tumors has been divided into 3 categories: benign, locally aggressive or borderline, and malignant. Because vascular tumors and other vascular anomalies may have unpredictable behavior, we suggest a multidisciplinary review of any suspected cardiac vascular anomaly (see the following section).

RECOMMENDED APPROACH TO EVALUATION AND TREATMENT OF A CHILD WITH A CARDIAC MASS.

The wide range of diagnoses and clinical manifestations of cardiac masses requires a comprehensive approach that takes into account the nature of the mass and the clinical context.[2] Echocardiogram is the initial imaging modality, allowing reliable diagnosis and treatment of typical cardiac rhabdomyoma and myxoma. CMR is recommended for all other mass types to determine the likely tissue type, define mass size and location, and evaluate its hemodynamic effect. The following CMR tissue characterization sequences are recommended: 1) cine SSFP imaging; 2) T_1-weighted black blood imaging; 3) fat-suppressed black blood imaging; 4) T_2-weighted black blood imaging; 5) first-pass perfusion imaging; and 6) LGE imaging. If a potential for malignancy or malignant behavior remains a concern, consider ^{18}F-FDG PET to assess for metabolic activity (Figure 6). Biopsy is considered when tissue diagnosis cannot be obtained by noninvasive means and the possibility of malignancy remains. Genetics consultation may identify genetic syndromes that are associated with the presence of a cardiac mass. Resection and/or debulking are considered when masses have 1 or a combination of the following features: 1) hemodynamic compromise; 2) life-threatening arrhythmias; and 3) risk of tumor-related thromboembolism (eg, myxoma, fibroelastoma). However, benign and malignant tumors may be unresectable because of the extent of involvement with key structures in and around the heart.

STUDY LIMITATIONS.

The retrospective nature of this investigation, with its requirements for CMR and a definitive diagnosis, limit the study's generalizability to all cardiac masses. In some cases, CMR imaging was modified with fewer tissue characterization sequences because the diagnosis was known before the study. Although parametric T_1 and T_2 mapping had been performed in several cases, sufficient data were lacking to make meaningful observations about the role of these sequences. Because many patients were referred from outside institutions, clinical treatment decisions and long-term follow-up data are limited, precluding analysis of the appropriateness of clinical management decisions. Because we encouraged the submission of rare mass types and limited inclusion to patients who had definitive diagnoses, the proportions of mass types in this study do not reflect their relative prevalence within the general pediatric population. Furthermore, because of their low prevalence, the accuracies of

the diagnostic features of several rare types of cardiac masses listed in Table 3 have not been validated.

CONCLUSIONS

CMR imaging of cardiac masses in children leads to an accurate diagnosis in the majority of cases, with a close association between a more comprehensive imaging protocol and a higher degree of diagnostic accuracy. Based on the findings in this cohort, we present updated diagnostic criteria for pediatric cardiac masses, with the addition of several types of rare tumors. This information may facilitate the diagnostic evaluation of children with this heterogeneous group of cardiac lesions (Central Illustration).

Supplementary Material

Refer to Web version on PubMed Central for supplementary material.

ACKNOWLEDGMENTS

The authors acknowledge the following individuals: David Annese, RT(R)(MR), Debi Wilkinson (case submission and processing), and Minmin Lu, MS (figure preparation).

ABBREVIATIONS AND ACRONYMS

^{18}F-FDG	^{18}F-fluorodeoxyglucose
CMR	cardiac magnetic resonance
LGE	late gadolinium enhancement
ISSVA	International Society for the Study of Vascular Anomalies
PET	positron emission tomography
SSFP	steady-state free precession

REFERENCES

1. Burke A, Virmani R. Pediatric heart tumors. Cardiovasc Pathol. 2008;17:193–198. [PubMed: 18402818]
2. Delmo Walter EM, Javier MF, Sander F, Hartmann B, Ekkernkamp A, Hetzer R. Primary cardiac tumors in infants and children: surgical strategy and long-term outcome. Ann Thorac Surg. 2016;102:2062–2069. [PubMed: 27344282]
3. Beroukhim RS, Prakash A, Valsangiacomo Buechel ER, et al. Characterization of cardiac tumors in children by cardiovascular magnetic resonance imaging a multicenter experience. J Am Coll Cardiol. 2011;58:1044–1054. [PubMed: 21867841]
4. Carreon CK, Sanders SP, Perez-Atayde AR, et al. Interdigitating myocardial tongues in pediatric cardiac fibromas: plausible substrate for ventricular tachycardia and cardiac arrest. J Am Coll Cardiol EP. 2019;5:563–575.
5. Fesslova V, Villa L, Rizzuti T, Mastrangelo M, Mosca F. Natural history and long-term outcome of cardiac rhabdomyomas detected prenatally. Prenat Diagn. 2004;24:241–248. [PubMed: 15065096]
6. Tworetzky W, McElhinney DB, Margossian R, et al. Association between cardiac tumors and tuberous sclerosis in the fetus and neonate. Am J Cardiol. 2003;92:487–489. [PubMed: 12914889]

7. Grebenc ML, Rosado-de-Christenson ML, Green CE, Burke AP, Galvin JR. Cardiac myxoma: imaging features in 83 patients. Radiographics. 2002;22:673–689. [PubMed: 12006696]

8. Mousavi N, Cheezum MK, Aghayev A, et al. Assessment of cardiac masses by cardiac magnetic resonance imaging: histological correlation and clinical outcomes. J Am Heart Assoc. 2019;8: e007829. [PubMed: 30616453]

9. Qin C, Shao F, Hu F, et al. ^{18}F-FDG PET/CT in diagnostic and prognostic evaluation of patients with cardiac masses: a retrospective study. Eur J Nucl Med Mol Imaging. 2020;47:1083–1093. [PubMed: 31807883]

10. International Society for the Study of Vascular Anomalies. ISSVA classification of vascular anomalies. Published 2018. Accessed October 30, 2020. https://issva.org/classification

PERSPECTIVES

COMPETENCY IN MEDICAL KNOWLEDGE:

Noninvasive techniques for the risk stratification of children with cardiac masses provide useful clinical guidance and, in some cases avert the need for biopsy. With robust tissue characterization sequences, CMR imaging is particularly useful in the noninvasive diagnosis of cardiac masses. We present data on 213 CMR studies of cardiac masses, all of which had a tissue or genetic diagnosis. Using previously defined diagnostic criteria, we evaluated the accuracy of 2 independent reviewers for the diagnosis of mass type. Of mass types that were represented in previously published diagnostic criteria (n = 174), both reviewers came to a single correct diagnosis in 70% of cases and to a correct diagnosis in 86% when ≤2 differential diagnoses were included. Because CMR for cardiac fibroma had a very high diagnostic accuracy (both reviewers with 94% single correct diagnosis), we propose that a diagnostic biopsy is not required when the following CMR characteristics of fibroma are identified: a large, intramyocardial mass that has a positive LGE pattern with patchy dark areas. Of 29 malignant tumors, both reviewers indicated malignancy in 52% (95% CI: 34%−70%) of cases as a single correct diagnosis and 83% of cases (95% CI: 69%−97%) when ≤2 differential diagnoses were included. Because of the clinical significance of an accurate diagnosis and its diverse and nonspecific CMR characteristics, we propose that when malignant tumor is considered, adding noninvasive measures (eg, ^{18}F-FDG PET) or tissue biopsy may be beneficial. New categories of cardiac masses were added to the diagnostic criteria, including fatty deposits in tuberous sclerosis, inflammatory myofibroblastic tumor, infectious/inflammatory masses, Rosai-Dorfman disease, benign myofibroblastic masses, hemangioendotheliomas, and vascular malformations. Information from this study may facilitate the diagnostic evaluation of children with this heterogeneous group of cardiac lesions.

TRANSLATIONAL OUTLOOK:

Cardiac masses in children are rare and encompass a wide range of tissue diagnoses and clinical behaviors. Much of the current medical knowledge in this field is limited to case reports and case series. Because the experience of individual centers is small, multicenter studies are paramount for the advancement of knowledge and treatment of these conditions. In this manuscript, we provide a detailed analysis of a large international collection of CMR studies of pediatric cardiac masses. We demonstrate that, although CMR characteristics are useful and may obviate the need for invasive biopsy, clinical features are also highly relevant to diagnosis and provide an incremental benefit over CMR characteristics alone. Included in this manuscript is a large series of malignant cardiac masses in children. Although a malignant diagnosis was associated with overall lower survival, our preliminary data documenting survival >4 years after diagnosis in several cases suggests that treatment of malignant masses may be effective in some situations. To further advance the field of pediatric cardiac masses, we must devote resources toward the development of a multicenter registry with a focus on diagnosis, management strategies, and long-term patient outcomes.

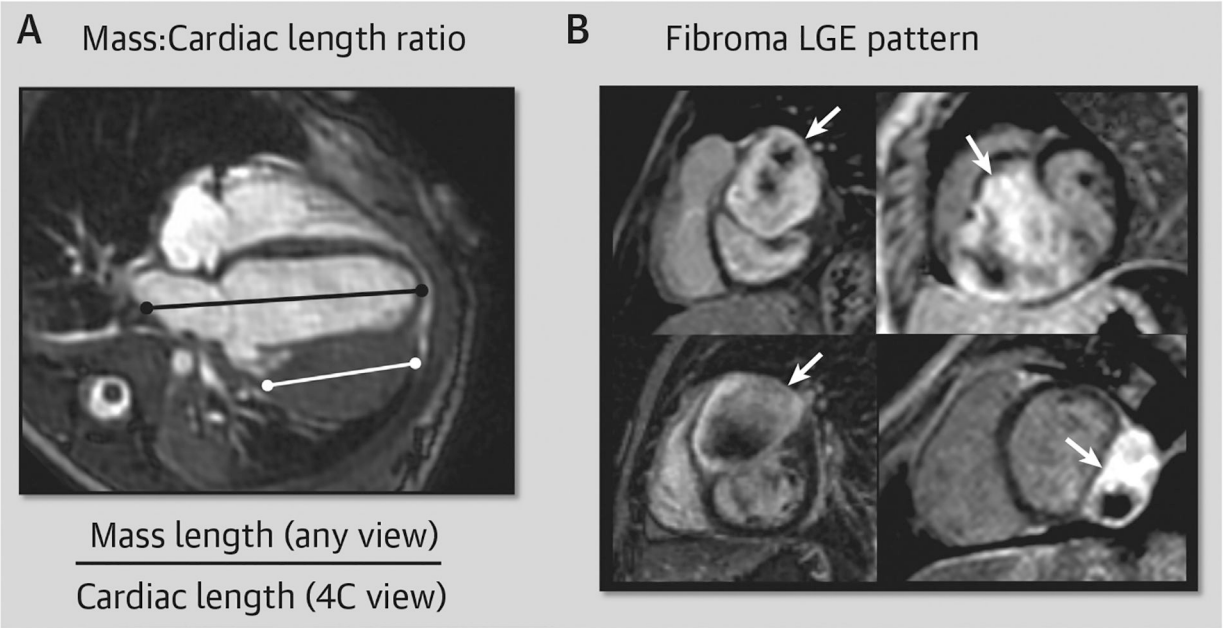

FIGURE 1.

Mass-to-Cardiac Length Ratio Measurement and Fibroma LGE Pattern

(**A**) The mass-to-cardiac length ratio measurement = largest mass length (in any view) ÷ cardiac length (4-chamber [4C] view). (**B**) A characteristic pattern of well-circumscribed hyperenhancement with patchy dark regions is commonly seen in fibromas (**white arrows**). LGE = late gadolinium enhancement.

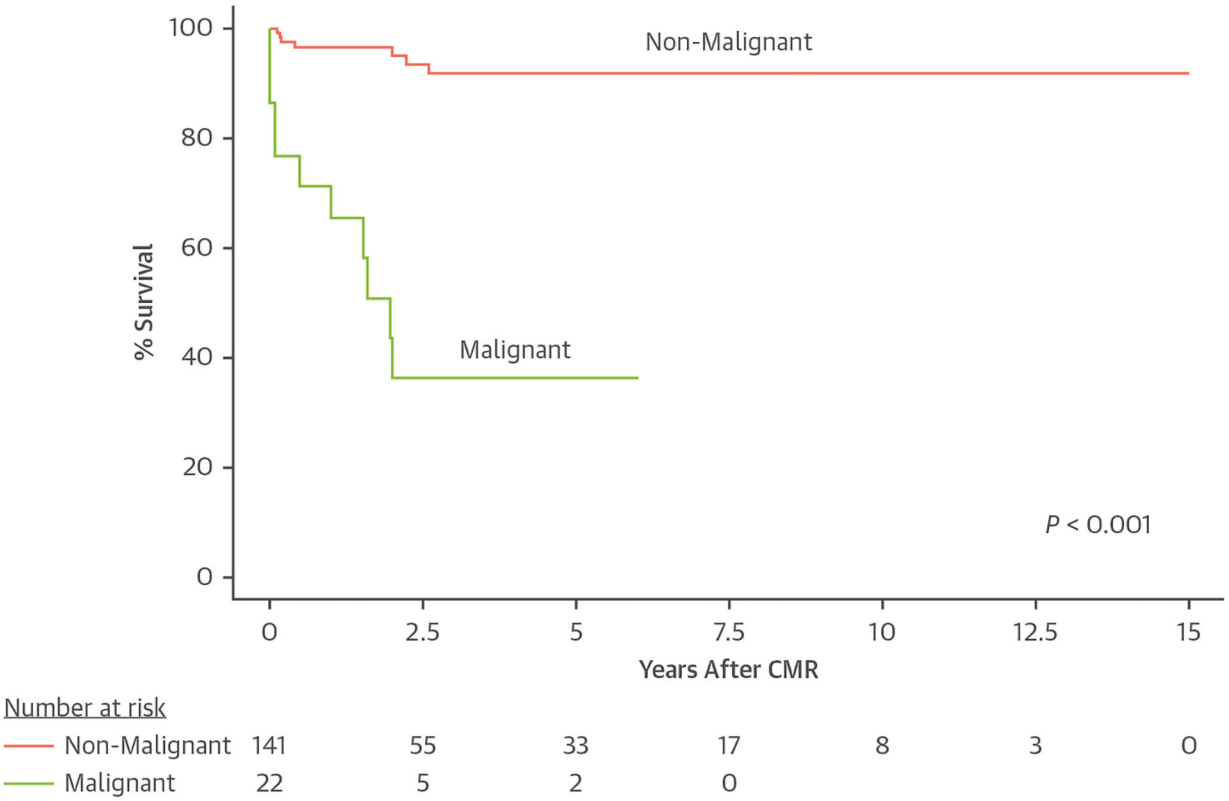

FIGURE 2.

Kaplan-Meier Estimates of Survival Following CMR Examination for Malignant and Nonmalignant Tumors

Lower survival was found for patients with malignant tumors ($P < 0.001$). CMR = cardiac magnetic resonance.

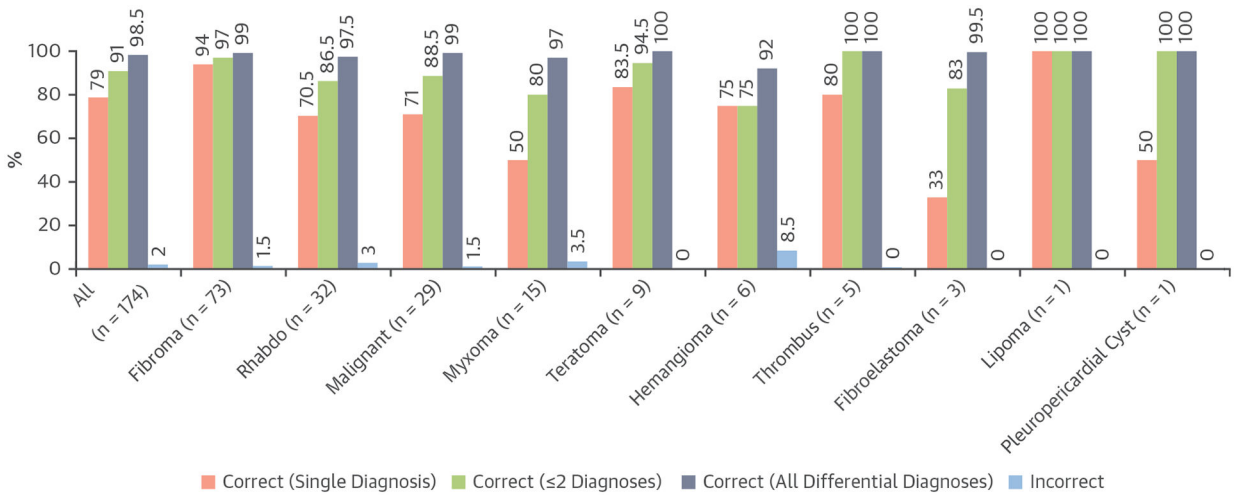

FIGURE 3.

Accuracy of the Original Diagnostic Criteria

Average diagnostic accuracy between 2 reviewers (single correct diagnosis, correct with ≤2 diagnoses, correct with all differential diagnoses, and incorrect diagnosis) for the 174 masses that were represented in the previously developed CMR diagnostic criteria. Rhabdo = rhabdomyoma; other abbreviation as in Figure 2.

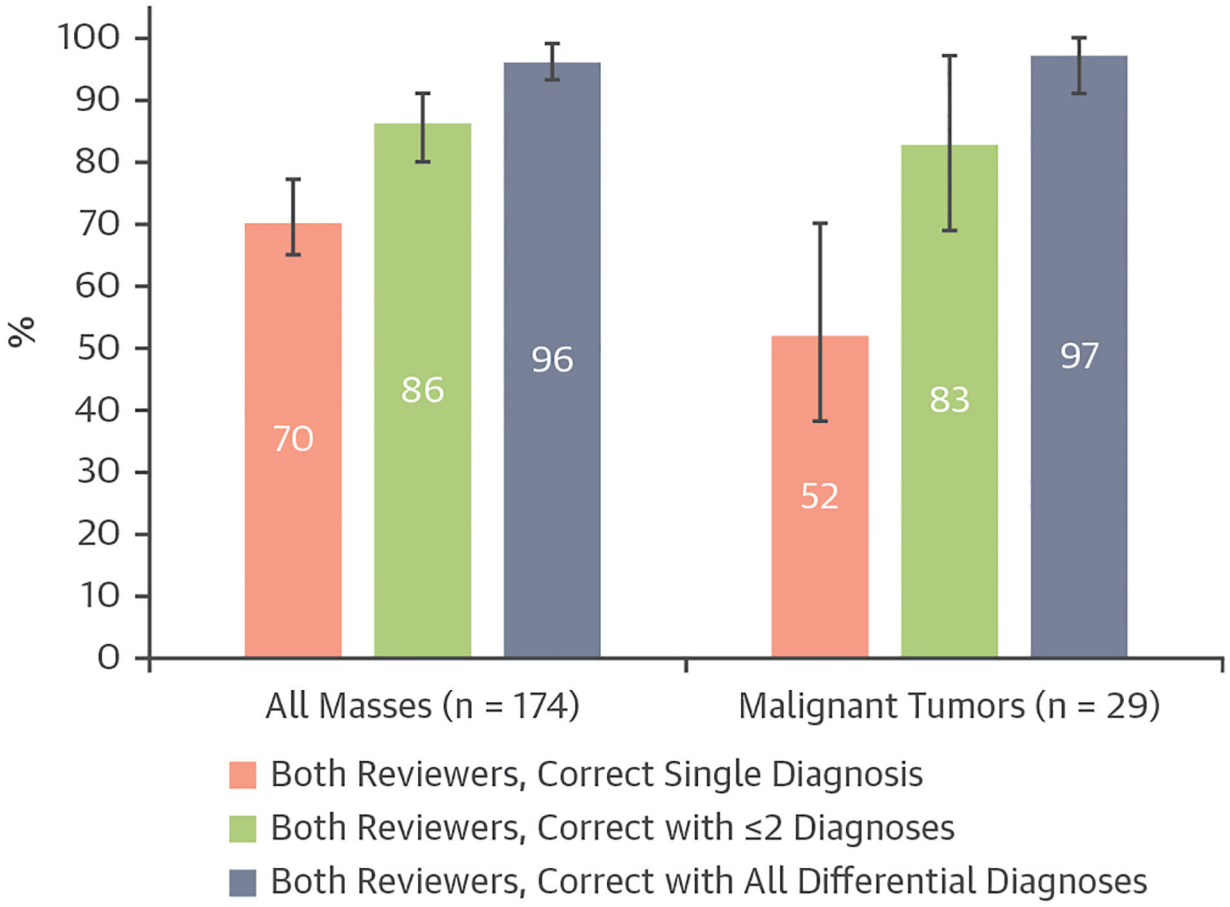

FIGURE 4.

Percent Diagnostic Agreement Between 2 Independent Reviewers

Bar graph demonstrating the percent diagnostic agreement between 2 independent reviewers with exact binomial 95% CIs, for all masses (including malignant tumors; n = 174) and malignant tumors (n = 29).

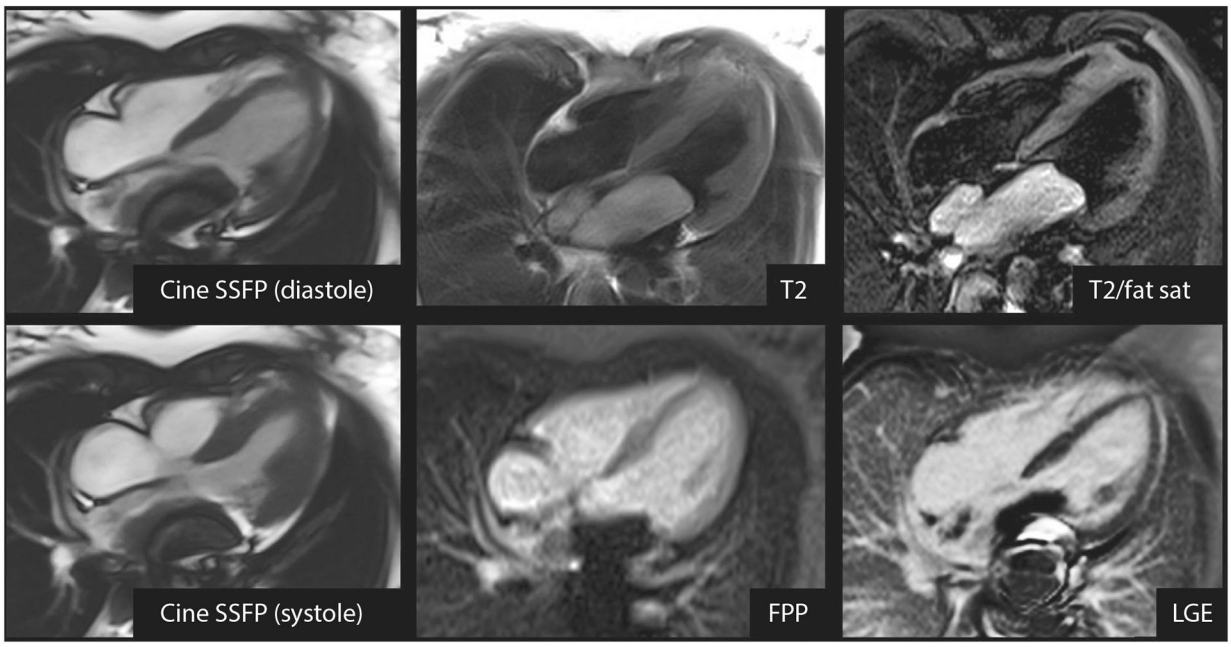

FIGURE 5.

High-Grade Leiomyosarcoma (Malignant Tumor) Incorrectly Diagnosed as a Myxoma

CMR of a 13-year-old child with palpitations and a large mass attached to the posterior wall of the left atrium, prolapsing through the mitral valve in diastole. Metallic susceptibility artifact obscures a portion of the mass. The mass is hyperintense on T_2-weighted imaging with and without fat suppression, does not enhance on FPP imaging, and does not enhance on LGE imaging. Reviewer 1 and the clinical CMR report indicated myxoma as a single diagnosis, whereas reviewer 2 indicated a differential diagnosis of myxoma, thrombus, and malignant tumor. FPP = first-pass perfusion; LGE = late gadolinium enhancement; SSFP = steady-state free precession; T2/fat sat = T2-weighted imaging with fat suppression; other abbreviation as in Figure 2.

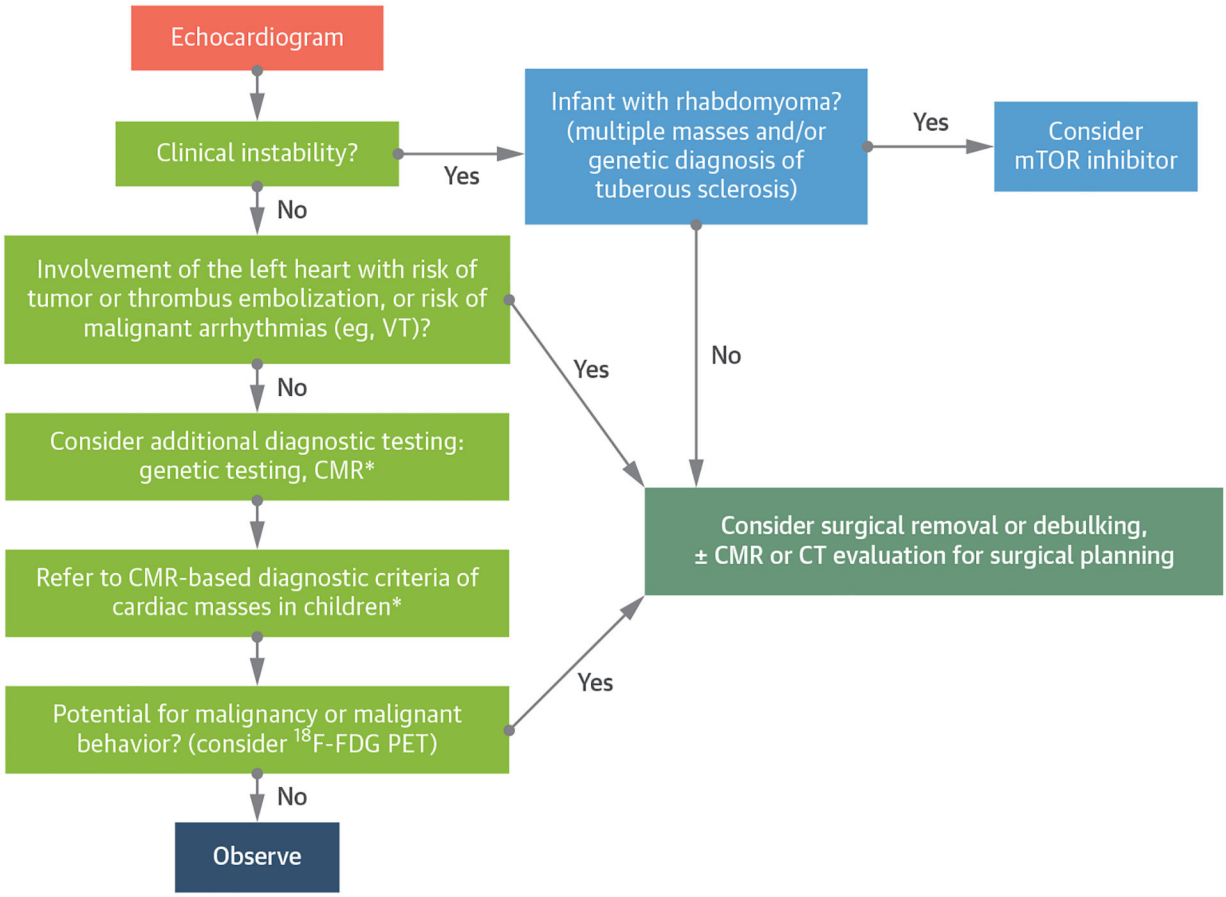

FIGURE 6.

Suggested Diagnosis and Management Algorithm for Pediatric Cardiac Masses

*See Table 3. ^{18}F-FDG = ^{18}F-fluorodeoxyglucose; CT = computed tomography; mTOR = mammalian target of rapamycin; PET = positron emission tomography; VT = ventricular tachycardia; other abbreviation as in Figure 2.

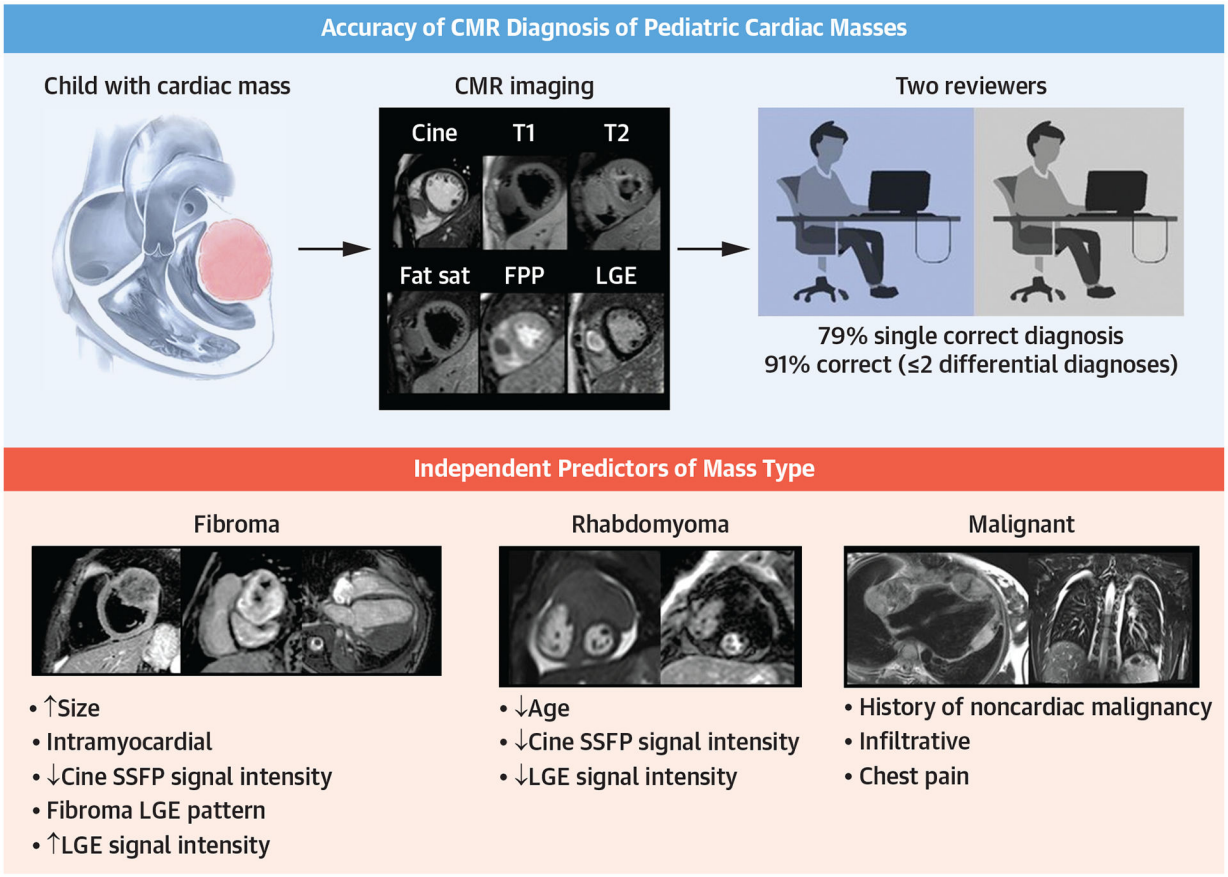

CENTRAL ILLUSTRATION.

Accuracy of CMR Diagnosis of Pediatric Cardiac Masses and Independent Predictors of Mass Type

We examined 213 CMR examinations of pediatric cardiac masses and tested the accuracy of previously developed diagnostic criteria[3] on 174 common masses that were represented in the diagnostic criteria. Independent predictors of mass type, including data from CMR tissue characterization sequences and clinical data, were identified for the most common masses by logistic regression. CMR = cardiac magnetic resonance; fat sat = fat suppressed; FPP = first-pass perfusion; LGE = late gadolinium enhancement; SSFP = steady-state free precession.

TABLE 1

Patient Demographic and Clinical Features

		Mass Type								
	All (N = 213)	**Fibroma (n = 73)**	**Rhabdomyoma (n = 32)**	**Malignant (n = 29)**	**Myxoma (n = 15)**	**Teratoma (n = 9)**	**Fatty Deposits in TSC (n = 7)**	**Hemangioma (n = 6)**	**Thrombus (n = 5)**	**Other (n = 37)**
Age at CMR, y	3 (0.4–12)	0.7 (0.3–5.4)	0.3 (0–1.5)	14 (8–17)	13 (8–15)	0.04 (0–0.2)	12 (12–15)	9.5 (4.5–14)	1.5 (0.9–3.7)	6.7 (3–13.4)
Male	111 (52)	37 (51)	14 (44)	14 (48)	5 (33)	4 (44)	5 (83)	5 (83)	4 (80)	21 (57)
Prenatal diagnosis	41 (19)	15 (21)	18 (56)	0 (0)	0 (0)	4 (44)	0 (0)	1 (17)	0 (0)	0 (0)
Genetic diagnosis[a]	51 (24)	11 (15)	27 (84)	0 (0)	4 (27)	0 (0)	7 (100)	0 (0)	0 (0)	2 (5)
History of malignancy	16 (7)	1 (1)	0 (0)	13 (43)	1 (7)	0 (0)	0 (0)	0 (0)	0 (0)	1 (3)
Respiratory symptoms	41 (19)	15 (21)	3 (9)	8 (28)	1 (7)	5 (56)	0 (0)	0 (0)	2 (40)	7 (19)
Arrhythmia	41 (19)	26 (36)	5 (16)	2 (7)	1 (7)	0 (0)	1 (17)	0 (0)	1 (20)	5 (14)
Murmur	31 (14)	15 (21)	3 (9)	1 (3)	3 (20)	0 (0)	0 (0)	1 (17)	2 (40)	6 (16)
Chest pain	17 (8)	3 (4)	0 (0)	8 (28)	1 (7)	0 (0)	1 (17)	0 (0)	1 (20)	3 (8)
Fever	13 (6)	0 (0)	0 (0)	4 (14)	1 (7)	0 (0)	0 (0)	0 (0)	1 (20)	7 (19)
Neurologic symptoms	13 (6)	2 (3)	3 (9)	2 (7)	2 (13)	0 (0)	1 (17)	0 (0)	0 (0)	3 (8)
Fatigue	8 (4)	1 (1)	0 (0)	3 (10)	0 (0)	0 (0)	0 (0)	2 (33)	0 (0)	2 (5)
Pericardial effusion	52 (24)	23 (32)	4 (13)	9 (31)	1 (7)	7 (78)	0 (0)	0 (0)	0 (0)	8 (22)
Pleural effusion	19 (9)	2 (3)	0 (0)	10 (34)	0 (0)	3 (33)	0 (0)	0 (0)	1 (20)	3 (8)
Hemodynamic impact[b]	79 (37)	23 (31)	12 (38)	13 (45)	4 (27)	9 (100)	0 (0)	1 (17)	1 (20)	14 (38)

Values are n (%) or median (IQR).

[a]Genetic diagnosis associated with mass type.

[b]Hemodynamic impact defined as inflow or outflow obstruction or the significant compression of cardiac or extracardiac structure.

CMR = cardiac magnetic resonance; TSC = tuberous sclerosis complex.

TABLE 2

Multivariable Logistic Regression Models of Diagnostic Features by Mass Type

Mass Type		OR	95% CI	*P* Value	Model C-Statistic
Multivariable models: CMR tissue characteristics					
Fibroma (n = 55/86)[a]	Cine SSFP intensity ratio			0.005	0.98
	High (>1.6)	Ref.			
	Medium (1.1–1.6)	12	2–72		
	Low (<1.1)	26	4–188		
	Fibroma LGE pattern	29	6–141	<0.001	
	LGE intensity ratio				
	Low (<1.4)	Ref.		0.007	
	Medium (1.4–4.2)	12	1–94		
	High (>4.2)	35	4–317		
	T_2 intensity ratio			<0.001	
	High (>1.7)	Ref.			
	Medium (1.1–1.7)	60	7–531		
	Low (<1.7)	37	5–270		
Rhabdomyoma (n = 22/143)[a]	Cine SSFP intensity ratio			0.005	0.93
	High (>1.6)	Ref.			
	Medium (1.1–1.6)	9	2–43		
	Low (<1.1)	9	2–39		
	LGE intensity ratio			<0.001	
	High (>4.2)	Ref.			
	Medium (1.4–4.2)	3	0.1–74		
	Low (<1.4)	113	7-NE		
Malignant (n = 24/146)[a]	T_2 intensity ratio			0.003	0.69
	Low (<1.7)	Ref.			
	Medium (1.1–1.7)	2	0.5–8		
	High (>1.7)	5	2–19		
Myxoma (n = 15/196)[a]	Cine SSFP intensity ratio			<0.001	0.83
	Low (<1.1)	Ref.			

Mass Type		OR	95% CI	*P* Value	Model C-Statistic
	Medium (1.1–1.6)	3	0.1–80		
	High (>1.6)	34	2–600		
Teratoma (n = 9/204)[a]	Cine SSFP intensity ratio			<0.001	0.80
	Low (<1.1)	Ref.			
	Medium (1.1–1.6)	0.3	0.01–9		
	High (>1.6)	6	1.01–36		
Hemangioma (n = 6/145)[a]	FPP intensity ratio ≥1	152	8-NE	<0.001	0.96
Multivariable models: all variables					
Fibroma (n = 59/106)[a]	Cine SSFP intensity ratio			0.004	0.99
	High (>1.6)	Ref.			
	Medium (1.1–1.6)	6	0.8–37		
	Low (<1.1)	36	4–302		
	Fibroma LGE pattern	9	2–43	0.004	
	LGE intensity ratio			0.010	
	Low (<1.4)	Ref.			
	Medium (1.4–4.2)	30	2–421		
	High (>4.2)	79	5-NE		
	Mass-to-cardiac length ratio >0.6	23	3–205	0.005	
	Intramyocardial	94	10–858	<0.001	
Rhabdomyoma (n = 22/143)[a]	Cine SSFP intensity ratio			0.012	0.97
	High (>1.6)	Ref.			
	Medium (1.1–1.6)	12	2–66		
	Low (<1.1)	12	2–81		
	LGE intensity ratio			<0.001	
	High (>4.2)	Ref.			
	Medium (1.4–4.2)	2	0.1–52		
	Low (<1.4)	188	10-NE		
	Age, y			0.008	
	High (>7)	Ref.			
	Medium (0.7–7)	30	1–610		
	Low (<0.7)	122	5-NE		

Mass Type		OR	95% CI	*P* Value	Model C-Statistic
Malignant (n = 24/146)[a]	History of malignancy	71	12–411	<0.001	0.94
	Infiltrative	37	10–137	<0.001	
	Chest pain	8	2–42	0.011	
Myxoma (n = 15/196)[a]	Endocardial	138	8-NE	<0.001	0.91
Teratoma (n = 9/204)[a]	Intrapericardial	606	22-NE	<0.001	0.97
	Age, y			0.020	
	High (>7)	Ref.			
	Medium (0.7–7)	4	0.1–134		
	Low (<0.7)	253	4-NE		
Hemangioma (n = 6/145)[a]	FPP intensity ratio ≥1	152	8-NE	<0.001	0.96

Each mass type has 2 separate multivariable logistic regressions with Firth adjustment for sparse data: 1) using 6 CMR tissue characterization sequences (see the “CMR Tissue Characteristics” section); and 2) using all clinical and CMR variables (see the “All Variables” section).

[a]The numerator represents the group whose characteristics are being examined, and the denominator represents the comparison group comprising all other tumors; numbers vary based on the number of studies with relevant tissue characterization sequences.

FPP = first pass perfusion; LGE = late gadolinium enhancement; NE = not estimable; OR = odds ratio; Ref. = reference; SSFP = steady-state free precession; other abbreviation as in Table 1.

TABLE 3

ses in Children

abdomyoma	Malignant	Myxoma	Teratoma	Fatty Deposits in TSC[a]	Thrombus
Muscular	Various	Endocardial	Ectopic tissue	Lipomatous	Other
<1–8	1–10	<1–9[b]	3–7	<1–5	1–2
• Intracavitary • Attached to LV or RV muscle • Can be atrium or epicardial • Usually multiple[c]	• Commonly SVC/IVC/RA • Epicardial, intrapericardial, anterior/posterior mediastinal • Infiltrative[d] • May cross tissue plane	• Typically left atrium but can be any chamber • Endocardial, pedunculated, mobile, heterogeneous • Mimics other masses: variable location and appearance	• Usually intrapericardial, compresses SVC/RA • Multilocular, bosselated, solid, and cystic areas • May be intramyocardial or intracavitary	• Intramyocardial • Commonly ventricular septum • Epicardial • Often multiple	• Intracavitary • SVC/IVC • Endocardial • Often in regions of stasis (lines, infarcts)
−	±	++	+	± (Rim of chemical shift artifact)	±
−	±	±	−	+	−
±	+	+	+	− (T_2/fat suppression)	−
No	No	No	No	Yes	No
−	±	−	−	−	−
−	±	±	±	−	±
Uncommon	Common	Uncommon	Common	No	Uncommon
• Usually diagnosed prenatally or in infancy • Tuberous sclerosis (>80% cases) • Atrial and ventricular arrhythmias	• Pleural effusion • Usually older children • History of malignancy • Chest pain • Multiple • High mortality • Metabolic activity on ^{18}F-FDG PET	• Usually older children • Greater prevalence in female patients • Triad of symptoms: (obstructive, constitutional, and systemic emboli) • Carney complex (30% CMR cases)	• Usually diagnosed prenatally or in infancy • Pericardial/pleural effusion • Respiratory symptoms	• Older children with tuberous sclerosis	• Dark on T_1 scout imaging • Dark on LGE sequence, long inversion time

Thrombus	• Various	• Fibroelastoma • Malignant	• Hemangioma • Pericardial cyst	• Lipoma	• Rhabdomyoma	

IMT	Rosai-Dorfman	Papillary Fibroelastoma	Benign Myofibroblastic Mass	Neurofibroma	Lipoma	Cyst
Endocardial	Histiocytic	Endocardial	Fibroblastic	Peripheral nerve sheath	Lipomatous	Malformation/ectopic tissue
<1–6	3–5	<1–2	1–2	5–8	1–5	1–5
Usually endocardial and intracavitary Can be intramyocardial or intrapericardial RA/RV more common Often polypoid, broad-based	• Variable	• Endocardial • Valve (usually mitral or aortic) • Pedunculated • Mobile	• Outflow tract • Well circumscribed	• Posterior mediastinal • Multiple	• Any location • Commonly intramyocardial or endocardial • May be valvular, pedunculated, mobile	• Pericardium • Posterior mediastinum (bronchogenic or foregut duplication cyst)
+	±	+	+	±	−	+
±	±	−	−	+	+	±
±	±	±	+	+	− (T_2/fat suppression)	++
No	No	No	No	No	Yes	No
−	−	±	−	−	−	−
Sometimes ++)	++	+	±	−	−	−
mmon in infants	Common	Uncommon	Uncommon	Uncommon	Uncommon	Common
ALK gene expression May be locally aggressive with recurrence and metastasis Heart murmur, fatigue Metabolic activity on ^{18}F-FDG PET/CT	• Neuro symptoms • Chest pain • Metabolic activity on ^{18}F-FDG PET	• Murmur • Embolic events	• Hemodynamic impact	• Older children • Neurofibromatosis • At risk for malignant degeneration	• Range of clinical presentations—usually benign, but may cause syncope or sudden death depending on location and risk of embolization	• Pericardial cysts may increase in size on repeat imaging

Low-grade sarcoma Myxoma Papillary fibroelastoma Inflammatory pseudotumor	• Infectious/ inflammatory	• Infectious/ inflammatory • Myxoma	• Papillary fibroelastoma	• Malignant
Hemangioma	**Angiosarcoma**	**Hemangioendothelioma**	**Vascular Malformation**	**Glomus tumor**
Vascular anomaly	Vascular anomaly	Vascular anomaly	Vascular anomaly	Vascular anomaly
1–6	6–9	3–6	5–10	<1–10
Any location, commonly RA during infancy Commonly inflow tracts Commonly endocardial Vascular channels	• Right atrium • Infiltrative • Extends to epicardium and anterior mediastinum • Rapid growth	• Right atrium • Left atrium • Occasionally ventricle • May be infiltrative with pericardial or mediastinal extension	• Solitary • Well circumscribed • Intramyocardial or epicardial • Heterogenous • Lymphatic malformation is commonly in RA, encasing a coronary artery	• Single or multiple intramyocardial masses
+	+	±	+	+
+	+	±	+	+
+	+	+	+	+
No	No	No	No	−
++	++	±	±	++
++	+	±	±	++
Infants	Common	Infants	Common	Common
Often incidental diagnosis Fatigue Fetal or neonatal presentation: pericardial effusion and tamponade	• Malignant • Metastatic • Older children • Chest pain • Fatigue • Dyspnea	• Range of behavior with malignant potential including metastasis (epithelioid hemangioendothelioma) • Fetal or neonatal presentation: pericardial effusion • Kasabach-Merritt phenomenon (consumptive coagulopathy) in kaposiform hemangioendothelioma	• May have arterial, capillary, venous, and/or lymphatic components • Resection may not be possible or may risk	• Resection may not be possible or may risk injury to cardiac structures • Usually found in the subungual regions of fingers and distal extremities (rare cardiac involvement)

JACC Cardiovasc Imaging. Author manuscript; available in PMC 2024 July 12.

	• Pleural effusion • High mortality • Metabolic activity on ^{16}F-FDG-PET	• Metabolic activity on ^{18}F-FDG-PET (described in noncardiac locations)	• injury to cardiac structures • Often respiratory symptoms, sometimes asymptomatic	• Usually benign, may be metastatic or have malignant potential
Teratoma (infants)	• Hemangioendothelioma	• Myxoma	• Pericardial cyst	• Hemangioma
Angiosarcoma	• Other malignancy	• Hemangioma	• Teratoma	• Hemangioendothelioma
Hemangioendothelioma		• Angiosarcoma		
Paraganglioma				

ense; ± indicates variable intensity; + indicates hyperintense; ++ indicates strongly hyperintense; and +++ very strongly hyperintense.

nd less likely to be located in the left atrium (referral bias).

al bias).

or crossing a tissue plane within the heart; 3) involving both cardiac and extracardiac structures; or 4) appearance of linear growth through a

na kinase; CT = computed tomography; IMT = inflammatory myofibroblastic tumor; IVC = inferior vena cava; LV = left ventricle; PET =
ntricle; SVC = superior vena cava; TSC = tuberous sclerosis complex; other abbreviations as in Tables 1 and 2.